Fig. S1. Repair of ICLs following a single or double replication fork collision. In the single fork model the collision of the fork with an ICL initiates a repair pathway that involves cleavage of the template strand for leading strand synthesis, and an additional incision, or exonucleolytic digestion (Wang et al., 2011), past the ICL, to complete unhooking of the template strands (Thompson and Hinz, 2009). Bypass synthesis across the ICL remnant is by extension of a parental template strand. In the dual fork collision model of the Walter group, replication forks are blocked on both sides of the ICL, triggering initiation of repair by unhooking and bypass synthesis, in this case by extension of a leading daughter strand (Raschle et al., 2008). In both models the broken fork is repaired by recombination, allowing resumption of replication.

Fig. S1

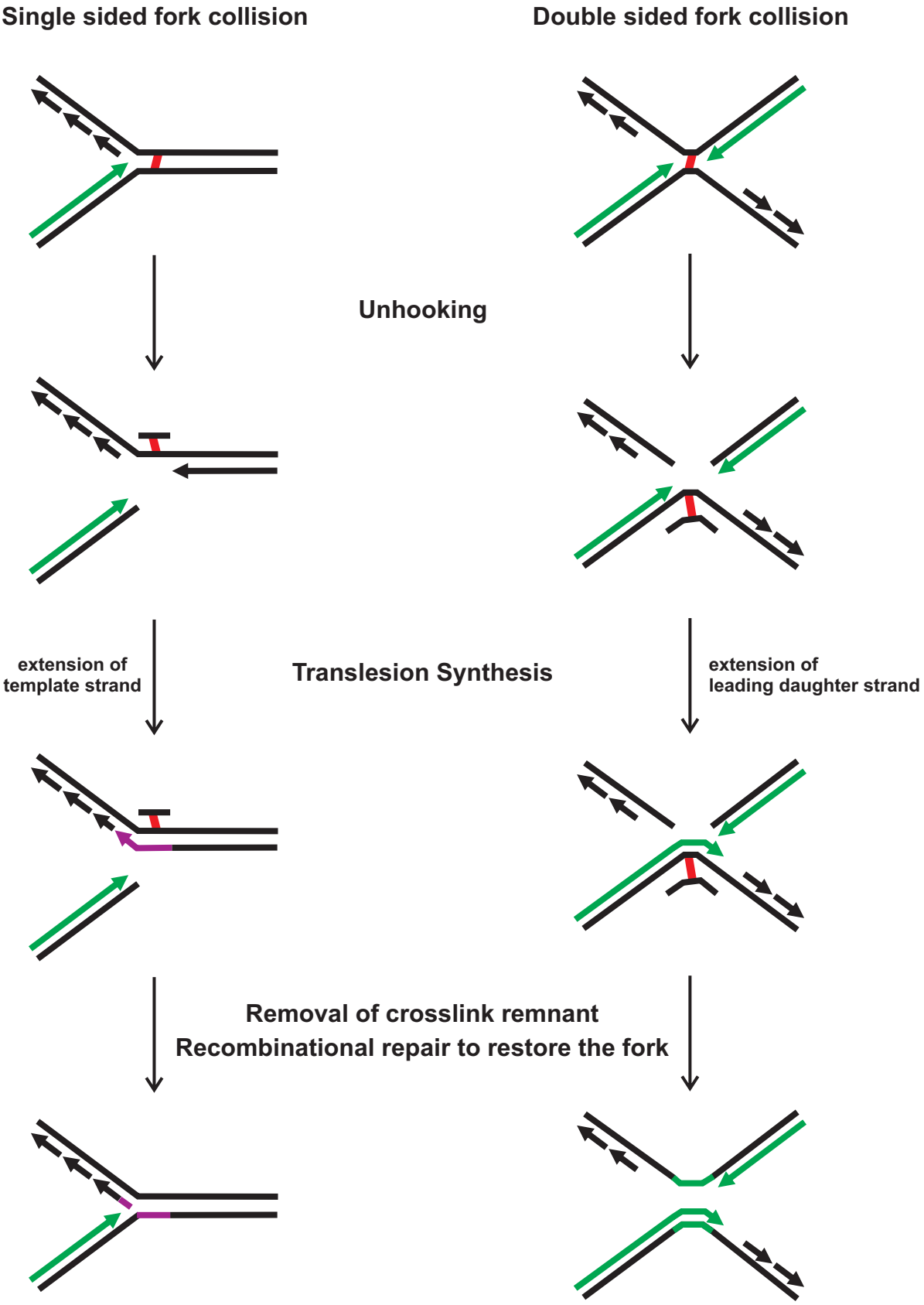
Single sided fork collision
Double sided fork collision
Unhooking
extension of
template strand
Translesion Synthesis
extension of
leading daughter strand
Removal of crosslink remnant
Recombinational repair to restore the fork

Fig. S2. Experimental outline and characterization of the ICL and MA products formed in a synthetic double stranded oligodeoxyribonucleotide standard by LC-MS/MS (Related to **Figure 1**)**.** A duplex oligodeoxyribonucleotide carrying a TA target sequence was treated with Dig-TMP/UVA to generate ICLs and MAs, and subsequently digested with nuclease P1 to generate the corresponding Dig-TMP ICL-tetranucleotide and Dig-TMP MA dinucleotide. Nuclease P1 digestion products were then analyzed by LC-MS/MS (see Experimental Procedures for more details).

On the left are depicted the negative-ion ESI-MS of the Dig-TMP ICL tetranucleotide (34.4 min peak (SIC), signature peaks (MS): $[M-3H]^{3-}$ m/z: 757.1 and $[M-2H]^{2-}$ m/z: 1136.0). The two bottom panels show the product-ion spectra (MS/MS) of the ESI-produced $[M-3H]^{3-}$ and $[M-2H]^{2-}$ ions of Dig-TMP-ICL-containing tetranucleotides. $[M-3H]^{3-}$ ion: shown in the inset is the selected-ion chromatogram (SIC) for monitoring the *m/z* 757.1→1096.4 transition for the Dig-TMP-ICL standard. $[M-2H]^{2-}$ ion: shown in the inset is the SIC for monitoring the *m/z* 1136.0→970.8 transition for the Dig-TMP-ICL standard.

On the right are shown the negative-ion ESI-MS of the Dig-TMP MA dinucleotide (38.7, 41.4, 43.3 min peaks (SIC), signature peaks (MS): $[M-2H]^{2-}$ m/z: 818.5 and $[M-H]^{-}$ m/z: 1637.8). The two bottom panels show the product-ion spectra (MS/MS) of the ESI-produced $[M-2H]^{2-}$ and $[M-H]^{-}$ ions of Dig-TMP-MA-containing dinucleotides. $[M-2H]^{2-}$ ion: shown in the inset is the SIC for monitoring the *m/z* 818.5→1557.9 transition for the Dig-TMP-MA standard. $[M-H]^{-}$ ion: shown in the inset is the SIC for monitoring the *m/z* 1637.8→1306.8 transition for the Dig-TMP-MA standard.

Fig. S2, Related to **Figure 1**

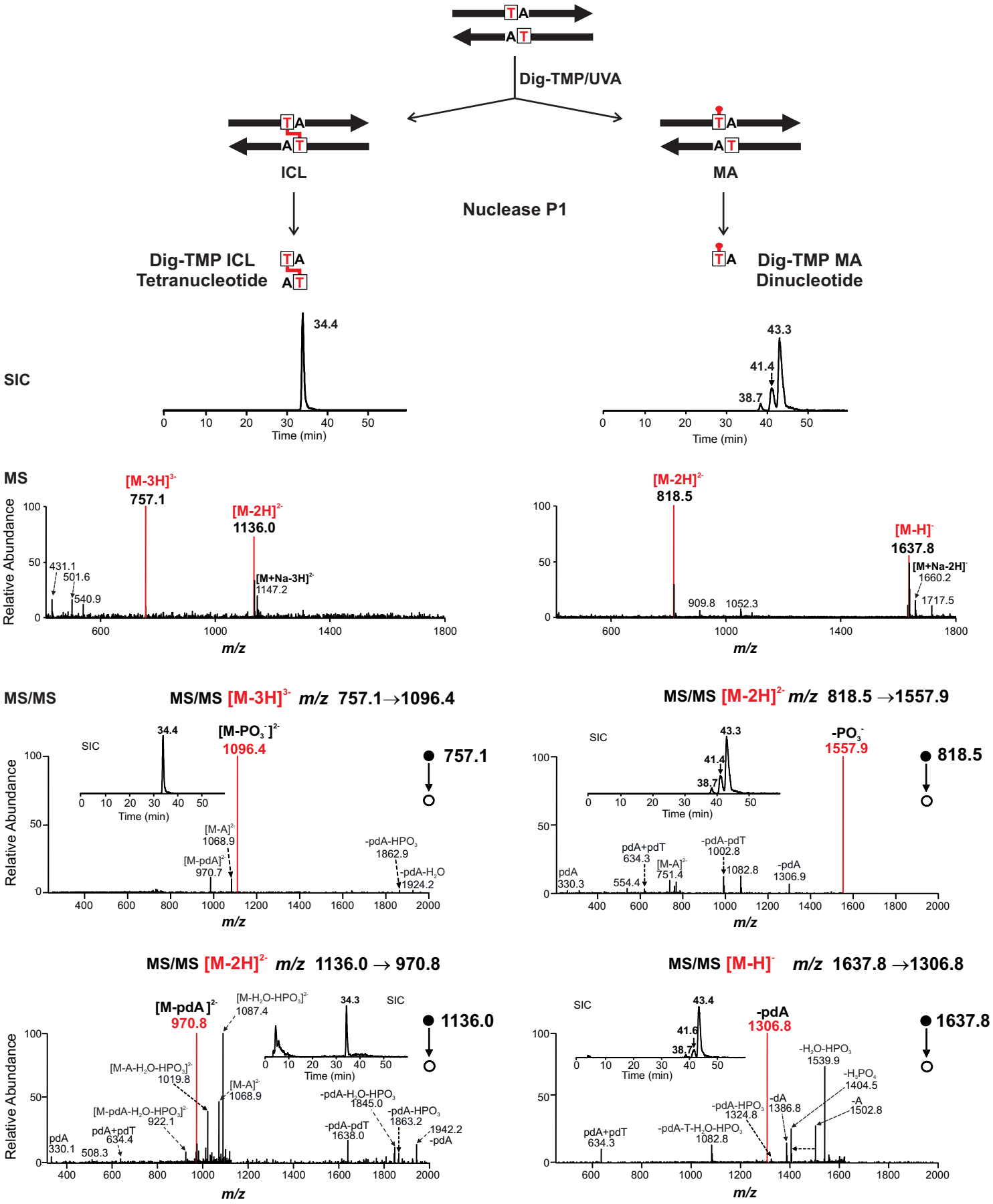

Fig. S3 (Related to **Figure 1**)**. A.** Structure of the Dig-TMP-ICL-containing tetranucleotide resulting from nuclease P1 digestion and the cleavages for the formation of major fragment ions observed in MS/MS (see Experimental procedures). **B.** Product-ion spectra of the ESI-produced $[M-2H]^{2-}$ ions of Dig-TMP-ICL-containing tetranucleotides from the nuclease P1 digestion of genomic DNA isolated from cells treated with Dig-TMP/UVA. Shown in the inset is the SIC for monitoring the *m/z* 1136.0→970.8 transition for the Dig-TMP ICL in genomic DNA. **C.** Product-ion spectra of the ESI-produced $[M-H]^-$ ions of Dig-TMP-MA-containing dinucleotides from the nuclease P1 digestion of genomic DNA isolated from cells treated with Dig-TMP/UVA. Shown in the inset is the SIC for monitoring the *m/z* 1637.8→1306.8 transition for the Dig-TMP-MA.

Fig. S3, related to **Figure 1**

A

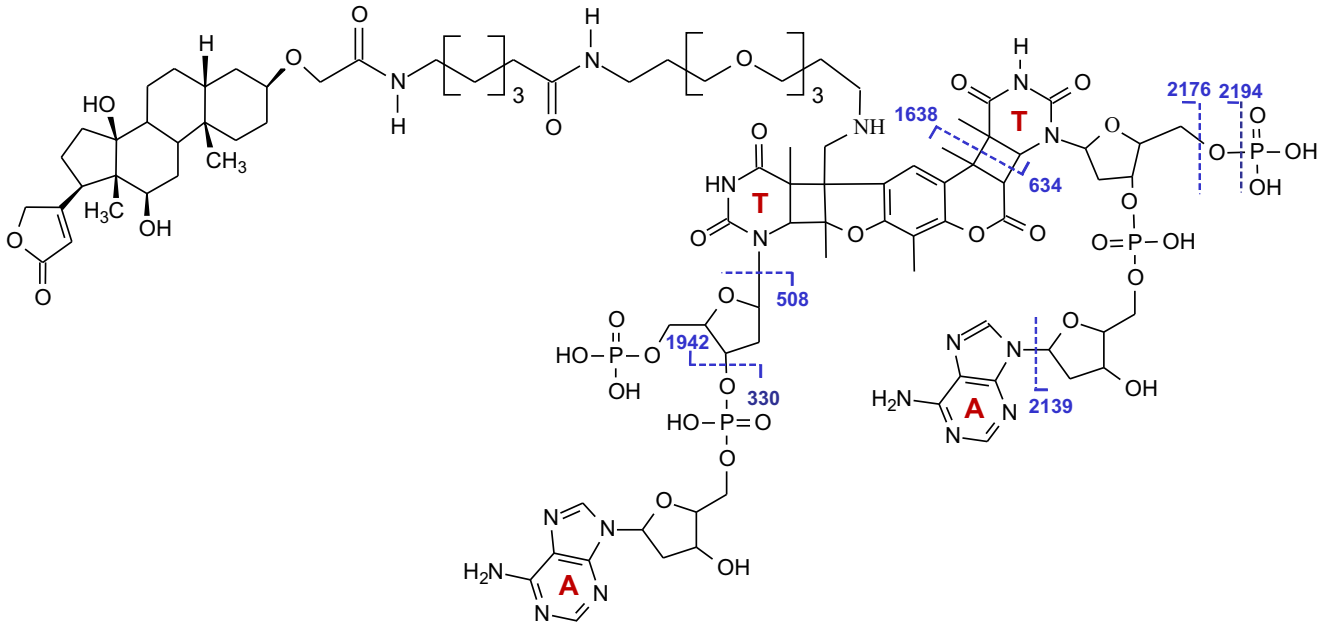

B

D-TMP ICL-tetranucleotide
Genomic DNA - D-TMP/UVA treated cells
MS/MS [M-2H]$^{2-}$ *m/z* 1136.0 → 970.5

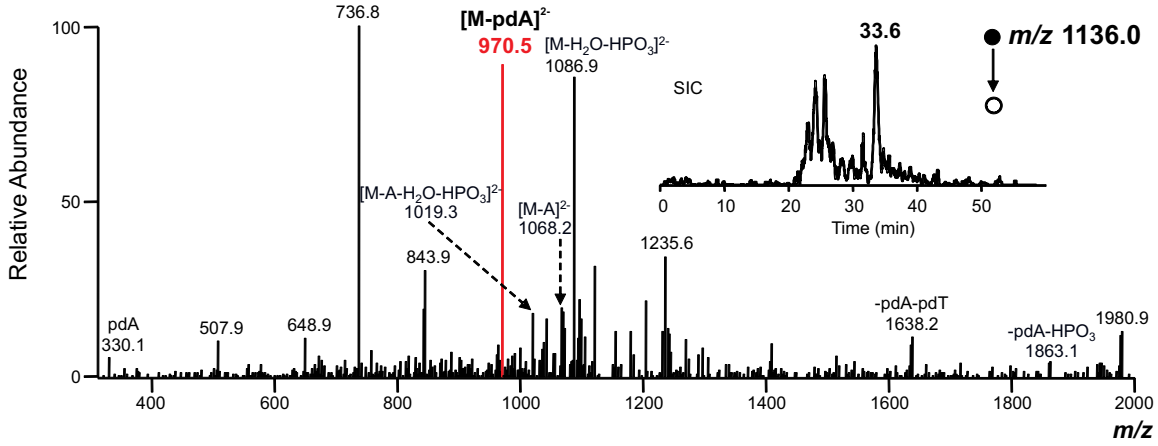

C

D-TMP MA-dinucleotide
Genomic DNA - D-TMP/UVA treated cells
MS/MS [M-H]$^{-}$ *m/z* 1637.8 → 1306.3

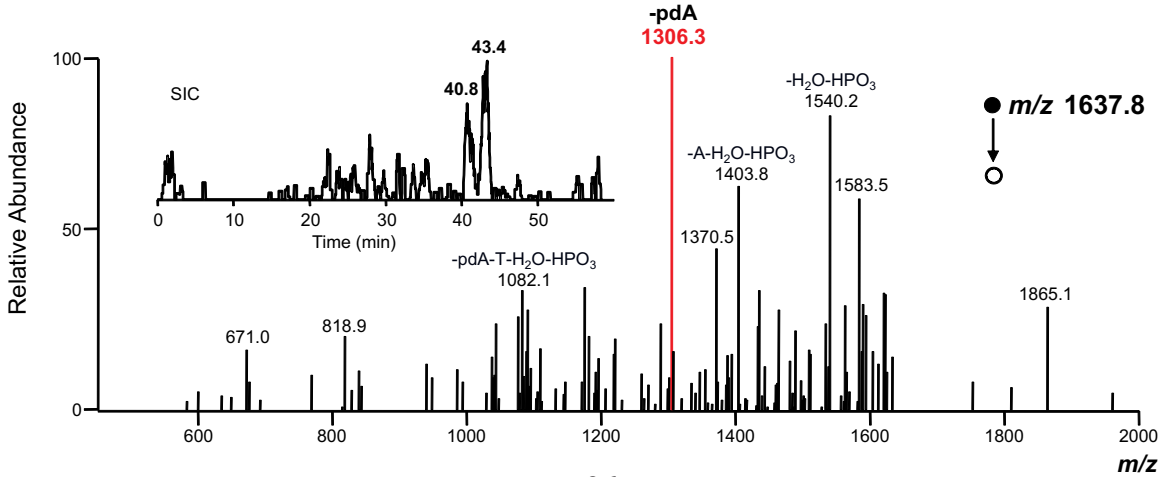

Fig. S4 (Related to **Figures 2 and 3**)**.**

A. Related to **Figure 2**: Image of a whole field of a single pulse experiment such as those depicted in Figure 2D,E,H,I. White arrows point to double sided events, whereas the arrowhead marks a single sided replication pattern.

B. Related to **Figure 3**: Image of a whole field of the triple color experiment depicted in Figure 3. Typically 1-10 EDU+ fibers were identified per field, and in some fields a few of these were also Dig+ [white arrows]. Two of the Dig+ fibers shown in this field are positive for the three labels EDU, CldU and IdU [ECI], whereas the third is only EDU-IdU(+) [EI].

Fig. S4: related to **Figures 2** (S4A) **and 3** (S4B)**.**

A Related to **Figure 2**.

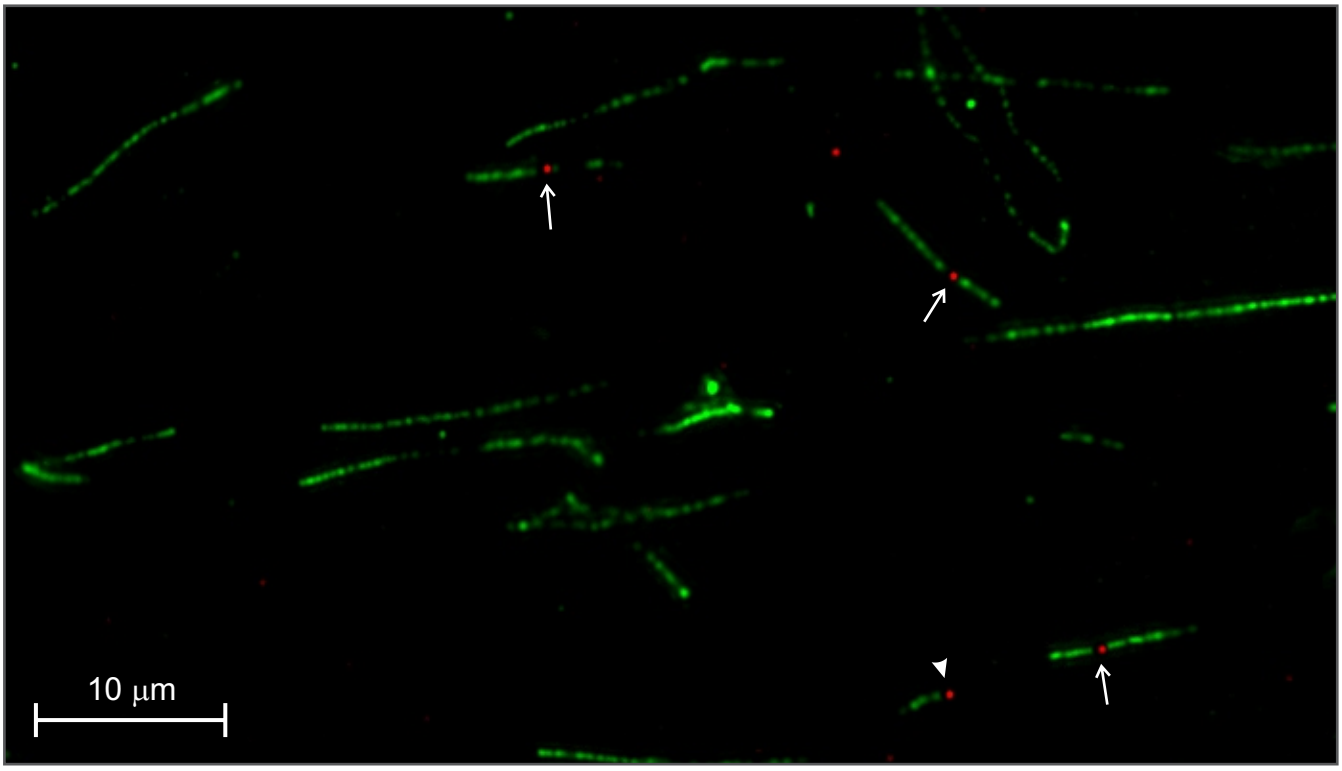

B Related to **Figure 3**.

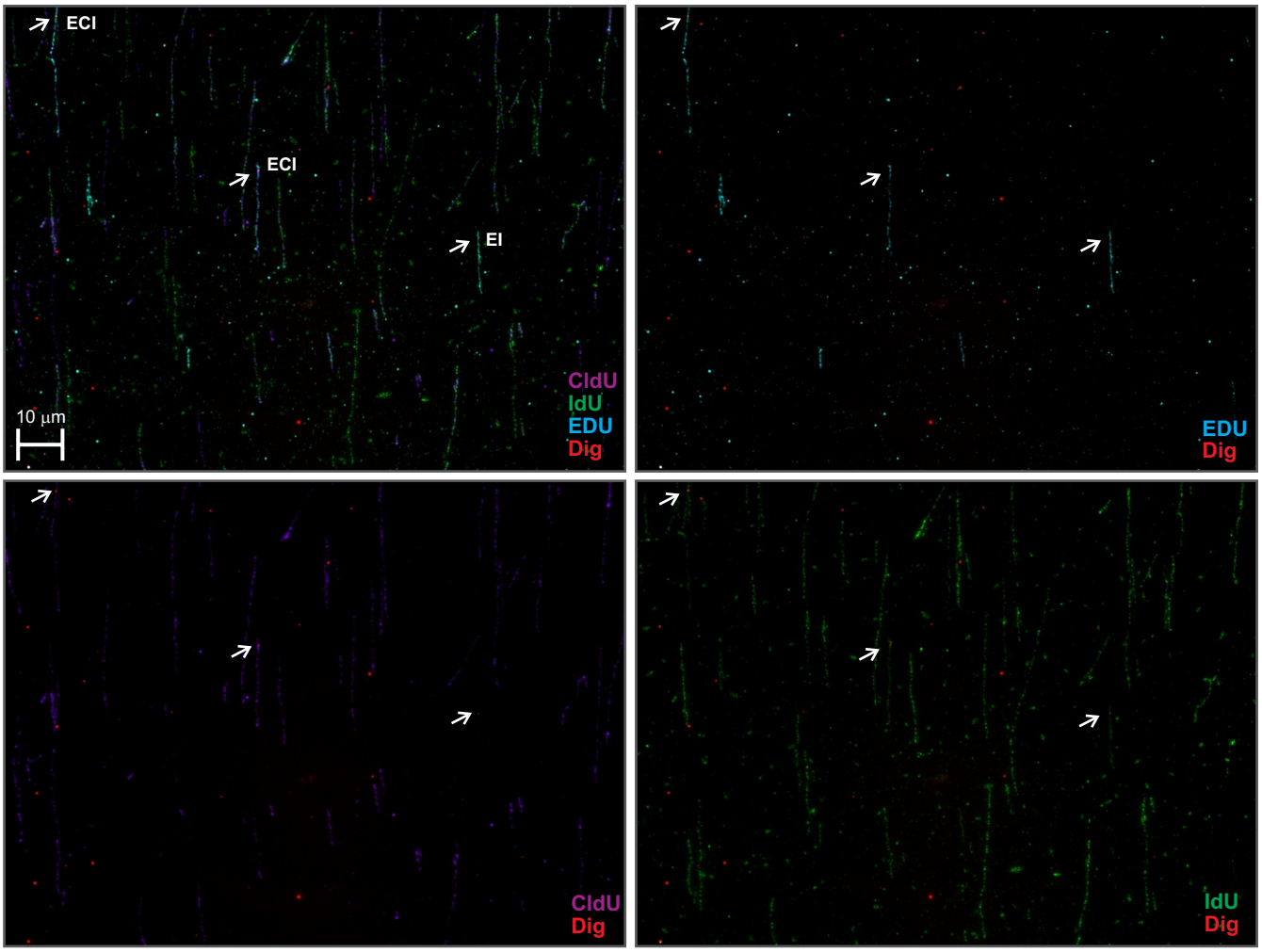

Fig. S5 (Related to **Figure 4**)**.**

A. Images of whole fields of a sequential pulse experiment (such as the ones described in Figures 4-6). White arrows point to fibers carrying a Dig signal.

B. Time cost of replication traverse in wild type DT40 cells and MEFs.

Fig. S5, related to **Figure 4.**

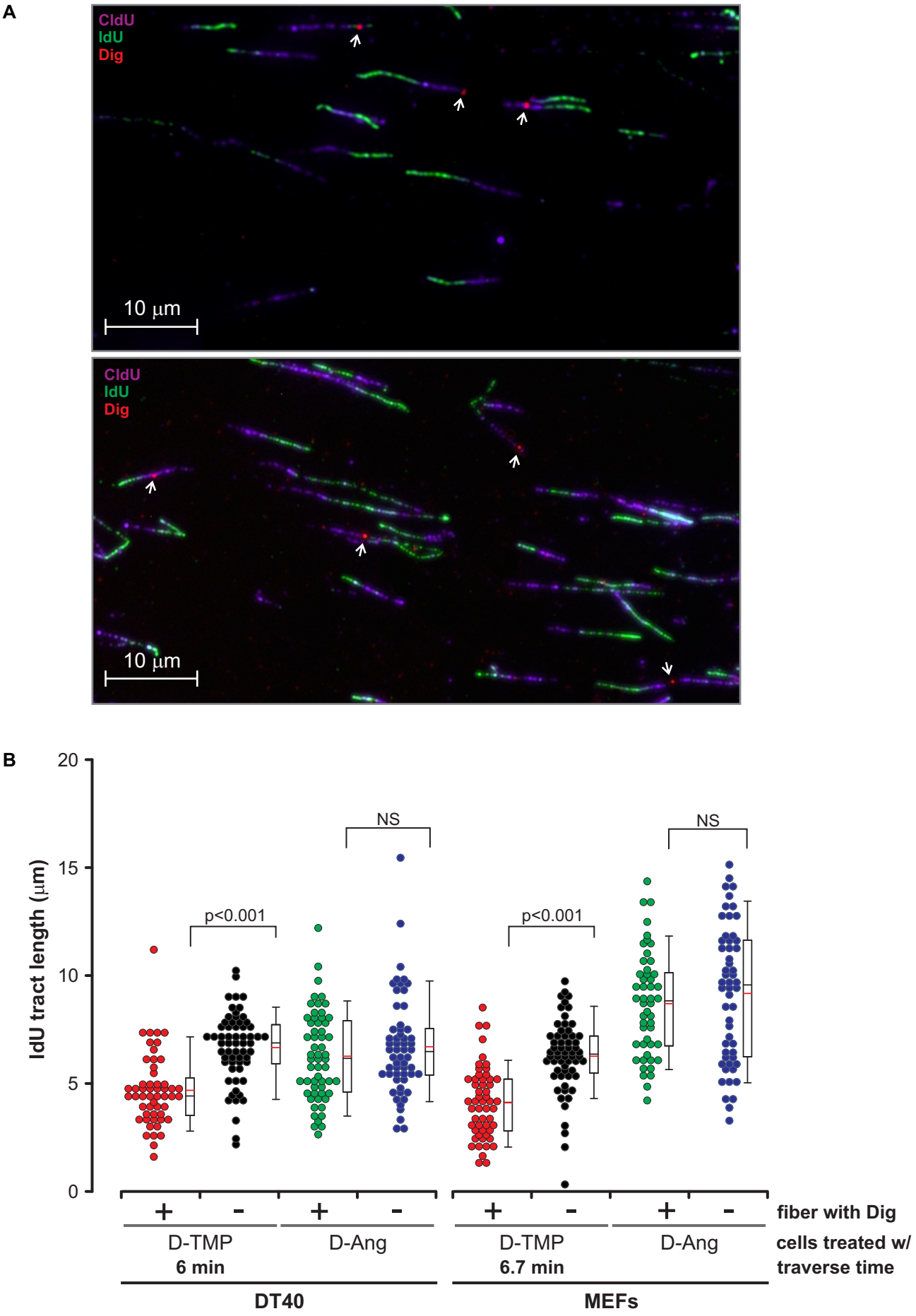

Fig. S6 (Related to **Figure 5**)**.**

A. The replication patterns described in Fig. 4E could be explained by dormant origin activation on the other side of the ICL stalling the replication machinery, as depicted in these schemes. In (**B**) the purple track stalls upon reaching an ICL. Activation of a dormant origin on the distal side of the ICL initiates bidirectional replication (still in purple). One of the forks will be stalled again at the ICL, whereas the one moving in the opposite direction will continue with the second label (green). **C-D** could be variations of B, reflecting differences in terms of timing of dormant origin firing with respect to the CldU and IdU pulses and fork stalling.

Fig. S6, Related to **Figure 5**

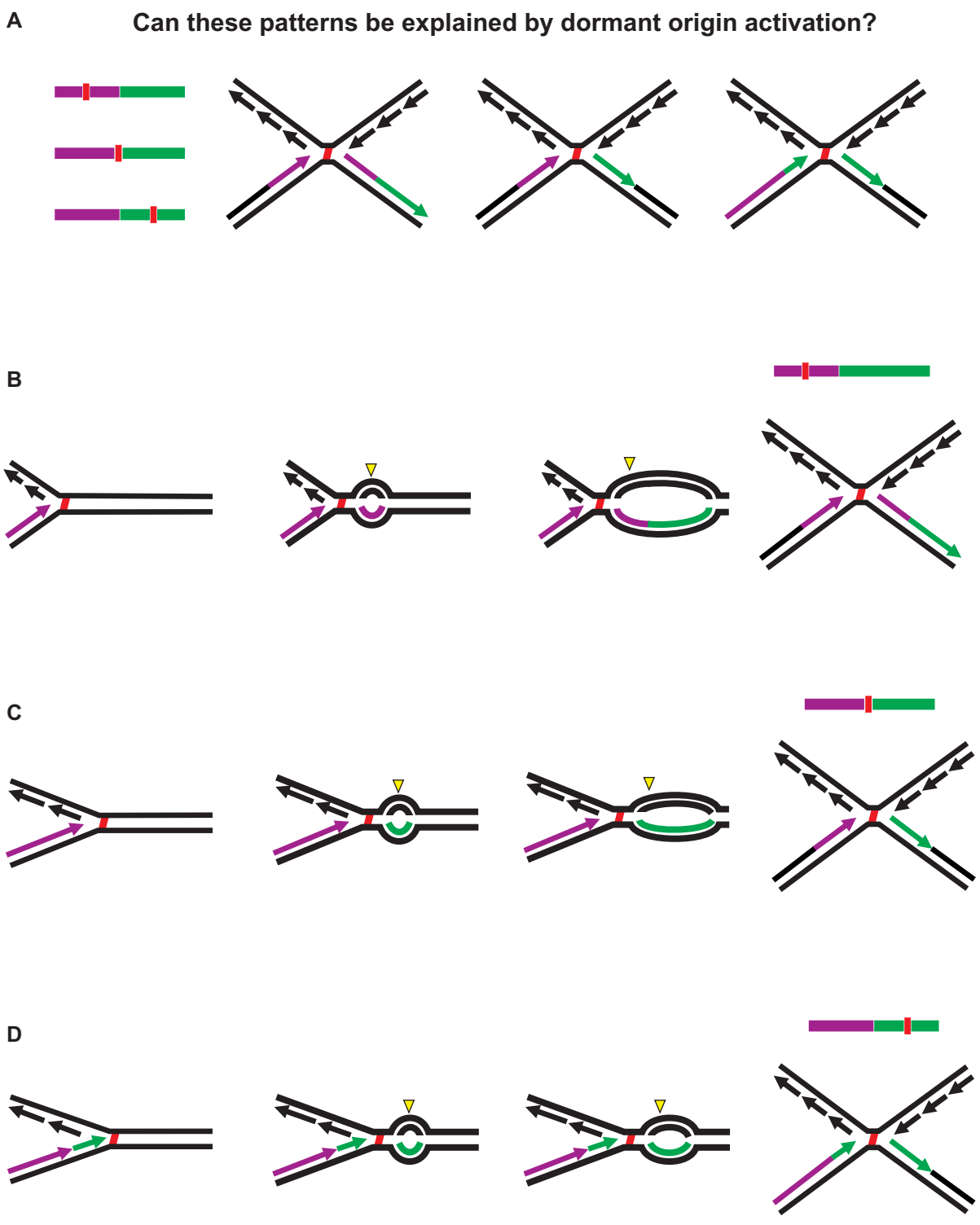

Fig. S7 Quantitation of replication patterns in mouse, human and hamster cell lines (related to **Figure 6**)**. A.** Replication fork traverse of ICLs is reduced in FANCM deficient mouse embryo fibroblasts. Mouse embryo fibroblast deficient in FANCM (Bakker et al., 2009) and wild type cells were treated with Dig-TMP/UVA, sequentially pulsed with CldU (40 min) and IdU (20 min), and replication patterns quantified as in Fig. 4. **B, C, D:** Characterization of patient derived FANCF deficient and wild type FANCF complemented cell line. Skin fibroblasts were established from FA patient EUFA121, group F. Stable, complemented, cell lines were constructed by expression of wild type FANCF linked to GFP. **B**. The deficient cells were arrested in G_2 phase following exposure to MMC, while the complemented line (clone 8) and the wild type control cell line VU1479 were not. **C**. Ubiquitination of FANCD2 is restored in EUFA121-F cells complemented by expression of Wt FANCF. EUFA121-F cells and clones 6-9 expressing FANCF-GFP were exposed to MMC and the ubiquitination of FANCD2 examined by western blotting. The parental EUFA121-F and clones 6 and 7 showed no ubiquitination of FANCD2, while clones 8, 9 were positive. EUFA121-F and EUFA121-F+FANCF-GFP clone 8 were used in the replication experiments shown in Fig. 6C. **D**. FANCF-GFP is localized to the nucleus in clone 8 cells **E:** Replication fork traverse of ICLs is not affected by deficiencies in FA core complex proteins FANCA, FANCE and FANCG. Patient derived cell lines deficient for FANCA and FANCE, and CHO *fancG*$^{-/-}$ cells, and the respective complemented cells were treated with Dig-TMP/UVA, sequentially pulsed with CldU and IdU, and replication patterns quantified as in Fig. 4.

A, E: Data are from three independent experiments, and presented as mean ±SD. ($p<0.001$, chi-square test).

Fig. S7, related to **Figure 6.**

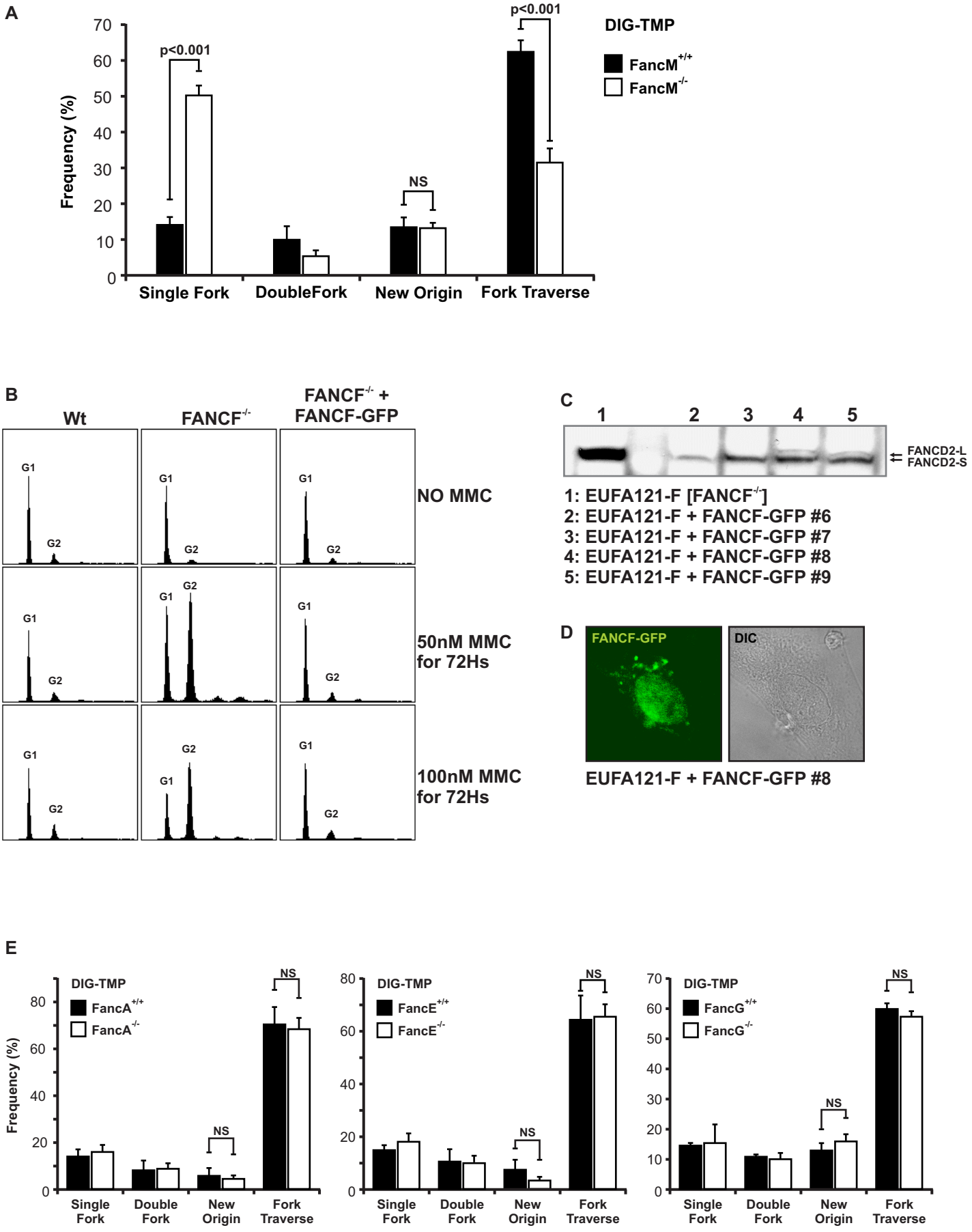

Supplemental experimental procedures

Alkaline comet assay

Cells were treated with 0.2 μM TMP and irradiated with UVA for 5 min, washed with PBS and scraped immediately, or placed in the incubator and harvested at different times after the UVA treatment. Cells were suspended in cold PBS and approximately 2×10^4 cells were mixed with 1.5% low-melting agarose and spread on a microscope slide that had been pre-coated with 1% agarose. Slides were placed in cold lysis buffer [2.5 M NaCl, 100 mM EDTA, 10 mM Tris (pH 7.5), 1% Triton X-100] overnight at 4°C, and rinsed three times in 1X PBS for 5 min. Slides were then incubated in cold unwinding solution [300 mM NaOH, 1 mM EDTA (pH 13)] in the dark at 4°C for 1 hour. Electrophoresis was carried out at 25 V for 45 min. Slides were rinsed in neutralizing solution [0.4 M Tris (pH 7.5)] three times for 5 min and fixed in 100% ethanol, before staining with ethidium bromide. Images of 50–100 cells per sample were obtained by using a fluorescence microscope (Axiovert 200 M, Carl Zeiss) and Axiovision 4.2 software. Individual comet images were evaluated by using Komet 5 image software. For the different time points the comet tail moment was normalized to the comet tail moment of mock treated cells (UVA only).

LC-MS/MS analysis of TMP adducts on EDU labeled replication tracts

10^9 ERCC1$^{-/-}$ cells were treated with 1 mM TMP, irradiated with UVA for 5 min, incubated with 10 mM EdU for 1 hour, washed with cold PBS and immediately harvested in cold PBS. The cells were lysed in 25 mM Tris-HCl pH 7.5, 100 mM EDTA, 1 % SDS, and nuclear DNA isolated by phenol extraction and ethanol precipitation. The

DNA was dissolved in 10 mM Tris-HCl pH 7.5 and the EdU analog was coupled to biotin through click reaction with 10 mM biotin-azide (Sirbu et al., 2012). The biotinylated DNA was ethanol precipitated again to remove free biotin, sonicated in a Bioruptor (Dyagenode) and captured on Dynabeads MyOne Streptavidin C1 magnetic beads (Invitrogen). The beads were washed three times in washing buffer (5 mM Tris-HCl pH7.5, 0.5 mM EDTA, 1 M NaCl, 0.1 % Triton-X), followed by one wash in 10 mM Tris-HCl pH 7.5. The EdU-Biotin-tagged DNA was subsequently released from the beads by nuclease P1 digestion and analyzed by LS-MS/MS to determine the relative abundance of ICLs and MAs in replicating DNA.

Preparation of chromatin extracts for MCM protein analysis

Cells were transfected and transfected again 24 hrs later with siRNAs. Forty eight hours after the second siRNA transfection cells were scraped, washed in cold PBS, suspended in 200μL buffer A (10 mM HEPES pH 7.9, 10 mM KCl, 1.5 mM $MgCl_2$, 0.34 M sucrose, 10% glycerol, 1 mM DTT, 10 mM NaF, 1 mM $NaVO_3$, 0.1% Triton X-100), and incubated on ice for 5 min. Nuclei were collected by centrifugation at 1,300 g at 4°C for 5min, washed once in buffer A, and then lysed in buffer B (3 mM EDTA, 0.2 mM EGTA, 1 mM DTT) for 10 min on ice. The insoluble chromatin fraction was collected by centrifugation at 1,700 g at 4°C for 5 min, washed once in buffer B, and spun down at 10,000 g at 4°C for 1 min. The isolated chromatin was resuspended in LDS sample buffer (Invitrogen), supplemented with 5 % 2-mercaptoethanol and sheared by sonication. In order to analyze total cellular proteins, whole cell extracts were prepared in RIPA buffer (10 mM Tris-HCl at pH 7.5, 1% Triton X-100, 0.1% SDS, 0.1% sodium deoxycholate, 140 mM NaCl, 1 mM EDTA). All buffers were supplemented with

complete protease inhibitor cocktail (Roche). SDS gel electrophoresis and Western blotting were performed according to standard procedures.

Supplemental References

1. Bakker, S.T., van de Vrugt, H.J., Rooimans, M.A., Oostra, A.B., Steltenpool, J., Delzenne-Goette, E., van der Wal, A., van, d., V, Joenje, H., te, R.H., and de Winter, J.P. (2009). Fancm-deficient mice reveal unique features of Fanconi anemia complementation group M. Hum. Mol. Genet. 18, 3484-3495.

2. Raschle, M., Knipsheer, P., Enoiu, M., Angelov, T., Sun, J., Griffith, J.D., Ellenberger, T.E., Scharer, O.D., and Walter, J.C. (2008). Mechanism of replication-coupled DNA interstrand crosslink repair. Cell 134, 969-980.

3. Sirbu, B.M., Couch, F.B., and Cortez, D. (2012). Monitoring the spatiotemporal dynamics of proteins at replication forks and in assembled chromatin using isolation of proteins on nascent DNA. Nat. Protoc. 7, 594-605.

4. Thompson, L.H., and Hinz, J.M. (2009). Cellular and molecular consequences of defective Fanconi anemia proteins in replication-coupled DNA repair: Mechanistic insights. Mutat. Res. 668, 54-72.

5. Wang, A.T., Sengerova, B., Cattell, E., Inagawa, T., Hartley, J.M., Kiakos, K., Burgess-Brown, N.A., Swift, L.P., Enzlin, J.H., Schofield, C.J., Gileadi, O., Hartley, J.A., and McHugh, P.J. (2011). Human SNM1A and XPF-ERCC1 collaborate to initiate DNA interstrand cross-link repair. Genes Dev. 25, 1859-1870.